Journal of Alloys and Compounds 508 (2010) 94–98

Contents lists available at ScienceDirect

Journal of Alloys and Compounds

journal homepage: www.elsevier.com/locate/jallcom

Thermal barrier coatings of rare earth materials deposited by electron beam-physical vapor deposition

Zhenhua Xu[a,b,c], Limin He[c,*], Xiaolong Chen[a,b], Yu Zhao[a,b], Xueqiang Cao[a,**]

[a] State Key Laboratory of Rare Earth Resource Utilization, Changchun Institute of Applied Chemistry, Chinese Academy of Sciences, Changchun 130022, China
[b] Graduate School of Chinese Academy of Sciences, Beijing 100039, China
[c] Beijing Institute of Aeronautical Materials, Department 5, P.O. Box 81-5, Beijing 100095, China

ARTICLE INFO

Article history:
Received 12 January 2010
Received in revised form 12 April 2010
Accepted 23 April 2010
Available online 5 May 2010

Keywords:
Thermal barrier coatings
Rare earths
Electron beam-physical vapor deposition
Gas turbine

ABSTRACT

Thermal barrier coatings (TBCs) have very important applications in gas turbines for higher thermal efficiency and protection of components at high temperature. TBCs of rare earth materials such as lanthanum zirconate ($La_2Zr_2O_7$, LZ), lanthanum cerate ($La_2Ce_2O_7$, LC), lanthanum cerium zirconate ($La_2(Zr_{0.7}Ce_{0.3})_2O_7$, LZ7C3) were prepared by electron beam-physical vapor deposition (EB-PVD). The composition, crystal structure, cross-sectional morphology and cyclic oxidation behavior of these coatings were studied. These coatings have partially deviated from their original compositions due to the different evaporation rates of oxides, and the deviation could be reduced by properly controlling the deposition condition. A double ceramic layer-thermal barrier coatings (DCL-TBCs) of LZ7C3 and LC could also be deposited with a single LZ7C3 ingot by properly controlling the deposition energy. $LaAlO_3$ is formed due to the chemical reaction between LC and Al_2O_3 in the thermally grown oxide (TGO) layer. The failure of DCL-TBCs is a result of the sintering-induced of LZ7C3 coating and the chemical incompatibility of LC and TGO. Since no single material that has been studied so far satisfies all the requirements for high temperature applications, DCL-TBCs are an important development direction of TBCs.

1. Introduction

In recent years, further increase in thrust-to-weight ratio and higher gas temperature are required in advanced turbine engines. In order to meet these requirements, ceramic thermal barrier coatings (TBCs) have been widely used in hot-section metal components in gas turbine either to increase the inlet temperature with a consequent improvement of the efficiency or to reduce the requirements for the cooling system [1,2]. The application of TBCs greatly enhances the operation temperature and thermal efficiency of gas turbines, and reduces fuel consumption and gas emission at elevated temperatures [1–4]. The selection of TBC materials is restricted by some basic requirements such as high melting point, low thermal conductivity, thermal expansion match with the metallic substrate, no phase transformation between room temperature and operation temperature, chemical stability, good adherence to the metallic substrate, and low sintering rate of the porous microstructure [5,6]. Typically, the TBC material presently used in gas turbines is partially stabilized zirconia containing 6–8 wt.% Y_2O_3 on a MCrAlY bond coat, deposited either by plasma spraying (PS) or by electron beam-physical vapor deposition (EB-PVD) [7]. A major disadvantage of yttria-stabilized zirconia (YSZ) is the limited operation temperature of 1473 K for long-term application. At higher temperatures, phase transformations from the t'-tetragonal to tetragonal and cubic ($t+c$) and then to monoclinic (m) occur, giving rise to the coating failure [8,9]. Moreover, the sintering-induced volume shrinkages would degrade the columnar structure of EB-PVD coatings and raise the elasticity modulus and, as a result, restrict the favorable strain tolerance of the coating [10].

In the next generation of advanced engines, further increases in thrust-to-weight ratio will require even higher gas temperature. This means that higher surface temperatures and larger thermal gradients are expected in advanced TBCs as compared with the conventional YSZ TBCs. Recently, some candidate materials for TBCs' application at higher temperature are under investigation, such as $LaMgAl_{11}O_{19}$, $La_2Zr_2O_7$ (LZ), 3 wt.% Y_2O_3–$La_2Zr_2O_7$, $La_2Ce_2O_7$ (LC) and $La_2(Zr_{0.7}Ce_{0.3})_2O_7$ (LZ7C3) [1–10]. Among the interesting candidates for TBCs, the rare earth zirconates and cerates (LZ, LC and LZ7C3) have been investigated and the results indicate that these materials show promising thermo-physical properties and have attracted a great attention [5].

It has been reported that LZ, LC and LZ7C3 coatings could be manufactured by PS method [5,8,11]. TBCs produced by EB-PVD have shown considerable improvement in tolerance to thermal cycling compared with those coatings made by PS [12]. The superior

* Corresponding author. Tel.: +86 10 62496456; fax: +86 10 62496456.
** Corresponding author. Tel.: +86 431 85262285; fax: +86 431 85262285.
E-mail addresses: he_limin@yahoo.com (L. He), xcao@ciac.jl.cn (X. Cao).

0925-8388/$ – see front matter © 2010 Elsevier B.V. All rights reserved.
doi:10.1016/j.jallcom.2010.04.160

Table 1
Chemical compositions of the as-deposited LZ, LC and LZ7C3 coatings.

Oxides	LZ		LZ7C3		LC	
	Theoretical value	Coating surface	Theoretical value	Coating surface	Theoretical value	Coating surface
La_2O_3 (wt.%)	56.9	59.47	54.16	58.18	48.63	51.49
ZrO_2 (wt.%)	43.1	40.53	28.68	23.19	–	–
CeO_2 (wt.%)	–	–	17.16	18.63	51.37	48.51

performance of EB-PVD coatings has been attributed to development of a feather-like columnar microstructure. Additionally, due to the large thermal expansion coefficient of LC, and the high sintering resistance of LZ7C3, it is a great hope that these materials will exhibit new-layered coatings with LZ7C3 coating on top of LC coating for good thermal protection. Hence it is necessary to investigate LZ, LC and LZ7C3 TBCs prepared by EB-PVD. Meanwhile, a double ceramic layer-thermal barrier coatings (DCL-TBCs) of LZ7C3 and LC could be deposited with a single LZ7C3 ingot by properly controlling the deposition energy, and their thermal cycling behaviors are also investigated.

2. Experimental

In the present study, rare earth oxide powders (La_2O_3, ZrO_2 and CeO_2) were heat-treated at 1273 K for 2 h in air before weighing as rare earth oxides are hygroscopic. Two ingot compositions (LZ and LZ7C3) were produced via a powder route by using rare earth oxides. After the cast-formation, the ingots were densified at 1773 K for 12 h.

The substrates (30 mm × 10 mm × 1.5 mm) were ground before bond coat (BC) of MCrAlY was deposited by arc ion-plating (A-1000 Vacuum Arc Ion-Plating Unit). BC has a nominal composition of 20–25Cr, 6–10Al, 0.08–0.4Y, 0.4–0.8Si, and Ni as balance (wt.%). The thickness of BC was in the range of 35–45 μm. After BC was deposited, substrates were heat-treated in high vacuum. The topcoats of rare earth zirconate or cerate coatings were deposited by EB-PVD and their thicknesses were about 100–200 μm. Electron beam current for deposition of zirconate and cerate coatings was in the range of 350–600 mA. Meanwhile, the accelerated high-voltage (kV) was in the range of −9.60 to −10.15. The deposition pressure of EB-PVD working chamber was about 7×10^{-3} Pa and no oxygen was introduced into the vacuum chamber. The average substrate temperature was 1098 ± 25 K and the rotation speed was 7 rpm.

The cyclic oxidation test of samples was heated in an air furnace at 1373 K for 30 min followed by removing out for cooling with airflow for 5 min. The heating-up and then cooling-down makes one oxidation cycle, and this process was repeated until 5% area of the ceramic coat was delaminated, and the cycling number was then regarded as the thermal cycling life of TBCs. The coating samples were embedded in a transparent cold-setting epoxy and then sectioned, ground and polished with diamond pastes down to 1 μm. Scanning electron microscope (SEM, FEI-Quanta 600) equipped with EDS (Oxford INCAx-sight 6427) was applied for the microstructure and composition evaluation. X-ray diffraction (XRD, Bruker D8 Advance) with Cu K_α radiation at a scan rate of $8^\circ\ min^{-1}$ was used for the phase determination of powders and coatings. Coatings without polishing were used directly for XRD measurement. In order to evaluate the lattice parameter, the silicon powder was used as the external standard.

3. Results and discussion

3.1. Composition and phase structure of the coatings

Partial decomposition of rare earth-zirconia (or -ceria) composite oxides ceramics could occur during EB-PVD due to different vapor pressures of the deposited oxides, which leads to composition derivation of the deposited ceramic coating from the original ingot [10,12,13]. In such case, it is necessary to optimize the chemical composition of original ingot and processing parameters for deposition of coating, in order to obtain the optimal phase with nearly stoichiometry composition. In this study, the optimized EB-PVD processing conditions were adopted for deposition of LZ, LZ7C3 and LZ7C3/LC (LZ7C3 on top of LC) DCL coatings. Chemical compositions of the as-deposited LZ, LC and LZ7C3 coatings are respectively listed in Table 1. Obviously, the ratio of two or three oxides in the as-deposited coatings analyzed by EDS has slightly deviated from the theoretical value after deposition. The contents of La_2O_3 and CeO_2 are higher in the coatings compared with the theoretical value. However, for the ZrO_2, the situation is just opposite. The possible reasons for these phenomena are: (1) the surface temperature of the ingot is very high during deposition, and different evaporation rates of the constituents might lead to the stoichiometry change when the material is heated; (2) from the calculation of Madelung energy of the pyrochlore structure ($A_2B_2O_7$), ZrO_2 is thermally more stable than La_2O_3 [14]; (3) the composition deviation seems to be a result of evaporation difference of CeO_2, La_2O_3 and ZrO_2 during deposition. Vapor pressures of the above oxides at 2773 K are 2×10^{-5} atm, 8×10^{-5} atm and 2×10^{-2} atm for ZrO_2, La_2O_3 and CeO_2, respectively [12,13]; (4) the amount of CeO_2 increase during deposition is higher than that of La_2O_3 (or ZrO_2) due to its high vapor pressure; (5) it exists a correlation between the chamber pressure and composition change during deposition [10,13]. The change in vapor pressure during deposition probably turns out to affect heavily the chamber pressure leading to deviate of composition. Additionally, the melting and evaporation behavior of the source material, ingot density, deposition rate and efficiency, gun power, e-beam focus, dwell time, melt pool, chamber pressure and vapor cloud geometry are predominant factors to control the coatings' composition during deposition [12,13].

On the other hand, there exists a correlation between deposition energy, vapor pressure and temperature during deposition [15]. When the ingot surface is heated by electron beam to a certain extent, the solid phase $La_2(Zr_{0.7}Ce_{0.3})_2O_7$ reaches firstly a molten state, and then attains a solid–liquid equilibrium, the gasification is finally initiated. Therefore, the chemical balance of $La_2(Zr_{0.7}Ce_{0.3})_2O_7$ can be expressed as:

$$La_2(Zr_{0.7}Ce_{0.3})_2O_7\,(s) = La_2O_3\,(g) + 0.6CeO_2\,(g) + 1.4ZrO_2\,(g) \quad (1)$$

According to the formula of Gibbs free energy, Eq. (2) is obtained when the reaction reaches the chemical balance:

$$\Delta G = -RT\ \ln(K_p) \quad (2)$$

In the above equation, ΔG is the free energy change ($kJ\ mol^{-1}$), K_p is the equilibrium constant, T is the temperature (K) and R is the gas constant ($J\ mol^{-1}\ K^{-1}$). Corresponding, their ΔG values can be roughly calculated to be $-47.9\ kJ\ mol^{-1}$, $-105.14\ kJ\ mol^{-1}$ and $-22.4\ kJ\ mol^{-1}$ for La_2O_3, CeO_2 and ZrO_2, respectively.

This calculation indicates that the absolute values of ΔG are in the order of $CeO_2 > La_2O_3 > ZrO_2$. In other words, when the ingot surface is heated by electron beam, evaporations of Ce and La are relatively faster than that of Zr. As a result, Ce and La decomposed from $La_2(Zr_{0.7}Ce_{0.3})_2O_7$ ingot can be selectively deposited when the deposition energy is properly controlled. After that, the evaporation of Zr is gradually achieved with the increase of deposition energy.

Additionally, the melting points for ZrO_2, CeO_2 and La_2O_3 are estimated to be ~3173 K, ~2673 K and ~2490 K, respectively, which indirectly proves that the deposition energy adopted for deposition of Zr is correspondingly higher than those of Ce and La. Therefore, these simple calculations give a qualitative explanation that DCL coating of LZ7C3/LC could be prepared by single LZ7C3 ingot with properly controlling the deposition energy. The composition analysis along the cross section of DCL coating by EDS is shown in Fig. 1, whose result is in good agreement with the explanations mentioned above.

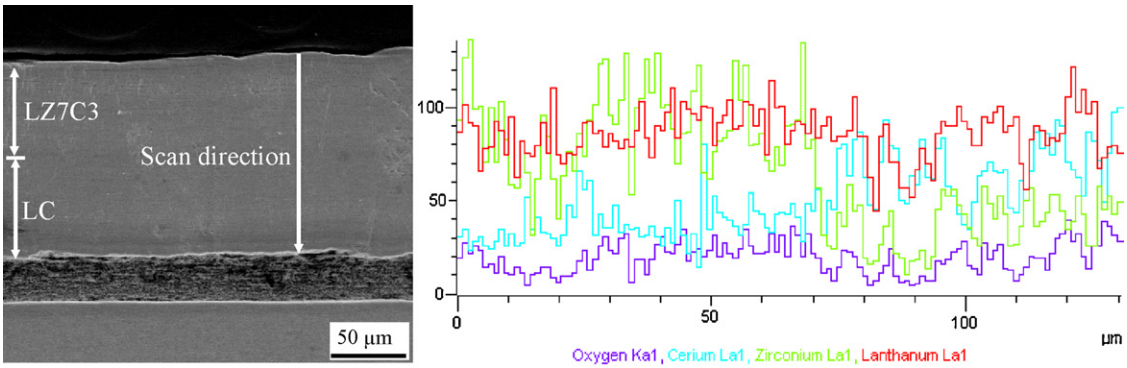

Fig. 1. SEM micrograph and EDS line scanning of DCL-TBCs.

Due to the fast cooling after deposition, before XRD experiment, three kinds of coating samples are heated in air at 1373 K for 20 h in order to improve the crystallization degree. Fig. 2a and b shows the XRD patterns of the as-deposited LZ coating and its original powder. It is obvious that the coating has a similar XRD pattern with its powder. It can be seen from Fig. 2b that the cubic pyrochlore structure is the main phase even though some La_2O_3 and t-ZrO_2 are also detected in the coating. It is also interesting to see that the peaks belonging to the pyrochlore structure slightly shift to the smaller 2θ-value (the larger d-values) compared with the starting powder. Meanwhile, the lattice parameter of the as-deposited LZ coating (10.822 Å) is larger than that of the theoretical value (10.793 Å) because the former has a higher content of La_2O_3 than the latter. La^{3+} (1.06 Å) has a larger ionic radius than Zr^{4+} (0.79 Å). The excess La_2O_3 in the coating is dangerous to the coating. It would absorb moisture from the air with the formation of $La(OH)_3$, leading to the swelling and then spalling of the coating. It was observed in our experiments that some LZ coatings with a high content of La_2O_3 spalled automatically after being stored for a few days. Therefore, the deposition condition of LZ coating should be properly controlled to keep the content of excess La_2O_3 as low as possible.

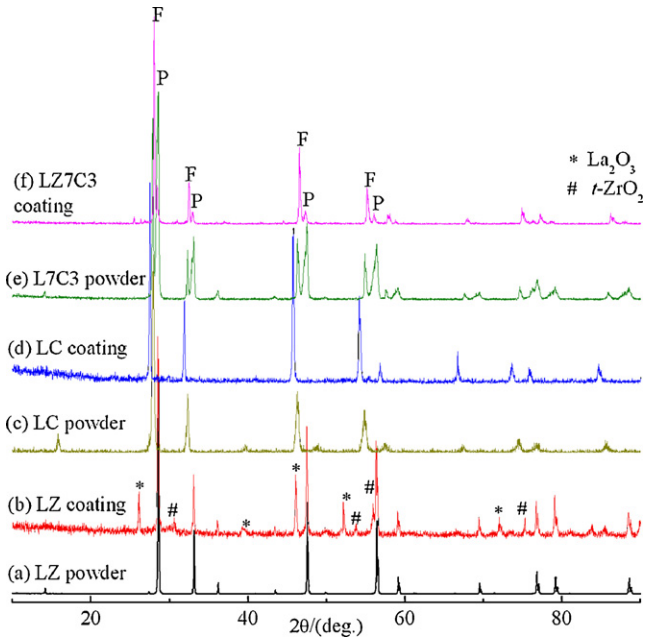

Fig. 2. XRD patterns of (a) LZ, (c) LC and (e) LZ7C3 powders, and the as-deposited coatings of (b) LZ, (d) LC and (f) LZ7C3. (*Note*: "F" and "P" represent "fluorite" and "pyrochlore" structures, respectively.)

On the other hand, in order to further prove the composition of DCL coating, the surface of DCL coating and the exposed LC coating after gradually grinding (No. 2500-SiC paper) of the coating layer by layer were analyzed by XRD. The distance after gradual grinding of the coating layer is measured by video microscope. The results obtained along the thickness of DCL coating are given in Fig. 2d and f. For comparison, XRD patterns of original powders of LC and LZ7C3 are also presented in Fig. 2c and e, respectively. It can be seen from Fig. 2c and d that LC coating has a very similar XRD pattern with its starting powder, implying that LC coating is deposited. It further proves that LC coating can be fabricated by properly adjusting the deposition parameters. This phenomenon is in good agreement with the result mentioned in Fig. 1. The cubic pyrochlore and fluorite structures are the main phases observed in Fig. 2e and f. For LZ7C3 powder, XRD peaks belonging to the pyrochlore structure are stronger than those of fluorite structure as shown in Fig. 2e. However, for the coating, the situation is opposite (Fig. 2f). It indicates that a solid solution of LC and LZ with fluorite structure is preferentially formed in LZ7C3 coating as compared with that of pyrochlore structure. Meanwhile, the preferred orientation growth of fluorite structure occurs in the ⟨0 0 1⟩ crystal direction. The reason may be that the different vapor pressures of La_2O_3, CeO_2 and ZrO_2 partially lead to the chemical composition deviation of LZ7C3 coating from that of the ingot during the EB-PVD process. It is also interesting to see that all the peaks (Fig. 2f) slightly shift to the larger 2θ-value (the smaller d-values) compared with the powder (Fig. 2e). The main reason is probably that the former has a higher content of CeO_2 than the latter, and Ce^{4+} (0.092 nm) has a smaller ionic radius than La^{3+} (0.106 nm).

3.2. Thermal cycling behavior of the coatings

The cross-sectional SEM images of the LZ, LZ7C3 and DCL coatings after thermal cycling test are presented in Fig. 3. After thermal cycling, a black thin layer with a thickness of 6–8 μm between the ceramic layer and BC is clearly observed in Fig. 3a and b, and this thin layer is so-called as the thermally grown oxide (TGO) layer, implying that BC oxidation is still an important factor for coating failure. The internal-oxidation of BC usually occurs by both the oxygen penetration through the inter-columnar gaps in the ceramic layer and oxygen-diffusion through the crystal lattice of the coating material [16]. Indeed, the degree of internal-oxidation of BC in LZ coating and the inhomogeneous morphology of TGO are significantly stronger than that of LZ7C3 coating as compared in Fig. 3a and b. The TGO layer consists of mainly Al_2O_3 and some oxides of Ni, Cr and Co as proved by EDS, which data is not shown in this paper. Differently, the TGO layer between LC coating and BC is not observed in Fig. 3c. The possible reason is that LC coating reacts with the TGO layer after such a long-term cycling. It indirectly indi-

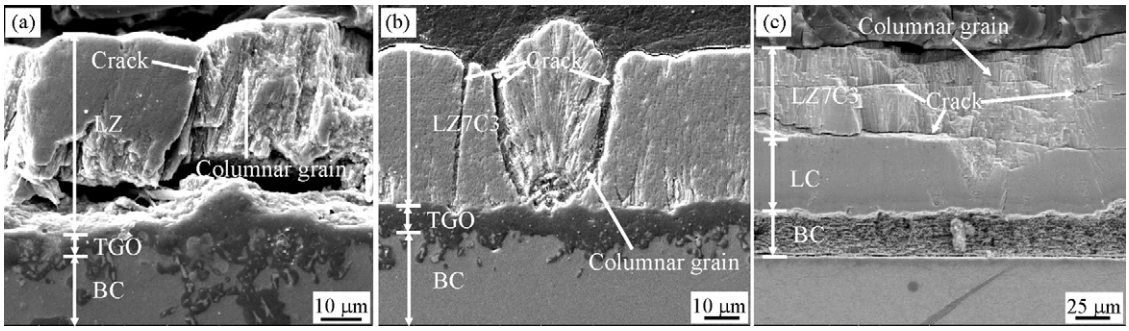

Fig. 3. Cross-sectional SEM images of LZ, LZ7C3 and DCL coatings after 588, 851 and 654 thermal cycles, respectively.

cates that the chemical compatibility of LC coating and TGO layer is unstable. In order to further study the stability of LC coating when it contacts TGO layer, a mixture of LC and Al_2O_3 in a molar ratio of 50:50 was heated at 1373 K for 48 h, and XRD results are shown in Fig. 4. After the heat-treatment, a new phase of $LaAlO_3$ is observed and only a little bit Al_2O_3 are detected in Fig. 4, and the possible reactions are following:

$$La_2Ce_2O_7 + Al_2O_3 = 2LaAlO_3 + 2CeO_2 \quad (3)$$

At high temperatures, $LaAlO_3$ can be formed due to the chemical reaction between LC and Al_2O_3, implying that LC is unstable at the application temperature of TBCs which is at least 1373 K after long-term cycling. This result further confirms that TGO layer is hardly observed as shown in Fig. 3c. $LaAlO_3$ has perovskite structure above 723 K and it undergoes a phase transformation to a rhombohedral symmetry when it is cooled, leading to the structure inhomogeneity [17,18].

The vertical cracks run through the ceramic layer, which are simultaneously observed in Fig. 3a and b and have further propagated down to BC surface. As a consequence, the occurrence of transverse cracks in BC surface causes the abnormal oxidation of BC and builds up growth stresses due to the volume swelling, which could reduce the adhesion strength of the interface between the ceramic layer and BC. As compared with LZ7C3 coating, the delamination of LZ coating from BC induced by transverse cracks is more serious, and one separation zone occurred between LZ coating and BC is more obvious (Fig. 3a). Additionally, its low thermal expansion coefficient and low fracture toughness are also responsible for spallation failure of LZ coating [5,10,19]. In this case, it is considered that air goes through those cracks to BC surface, and causes the abnormal oxidation of BC [20]. Therefore, a transverse (or vertical) crack is developed when the stress (i.e. thermal stress) is accumulated to some extent, leading to the initiative spallation of ceramic layer in TBCs. On the other hand, as shown in Fig. 3c, some transverse cracks are formed not only at the interface between LZ7C3 and LC coatings, but also inside LC7C3 coating. Part of LZ7C3 coating spalled from above (or near) the LC surface is also observed in Fig. 3c, and the spallation of DCL coating is layer by layer in LZ7C3 coating. It is concluded that the failure of DCL coating may start at the surface of LZ7C3 coating. The reason is that the surface temperature of LZ7C3 top coat is higher than that of LC bottom coat, and the sintering-induced effect of LZ7C3 coating surface occurs after long-term thermal cycling probably due to the elemental interdiffusion between these two coats induced by concentration gradient, which results in parallel contraction of LZ7C3 coating surface. On the other hand, one explanation for the occurrence of microcracks could be attributed to the reduction–oxidation of cerium oxide. The LZ7C3 ingot is heated in vacuum by electron beam source during deposition which is a reduced atmosphere and the cerium oxide is reduced to Ce^{3+} to a certain extent. When the reduced cerium oxide is annealed in air, it would be oxidized and the coating would swell. Therefore, the microcracks are easy to be formed due to the presence of cerium in both Ce^{3+} and Ce^{4+} oxidation states within LZ7C3 coating. In addition, the LZ and LZ7C3 coatings still keep columnar structure even after long-term thermal cycling (Fig. 3a–c), which is a typical and characteristic feature of the coating made by EB-PVD. This phenomenon further confirms that the LZ and LZ7C3 coatings still have a low sintering ability to a certain extent. Namely, the rare earth zirconates and cerates are candidate materials for TBCs' application.

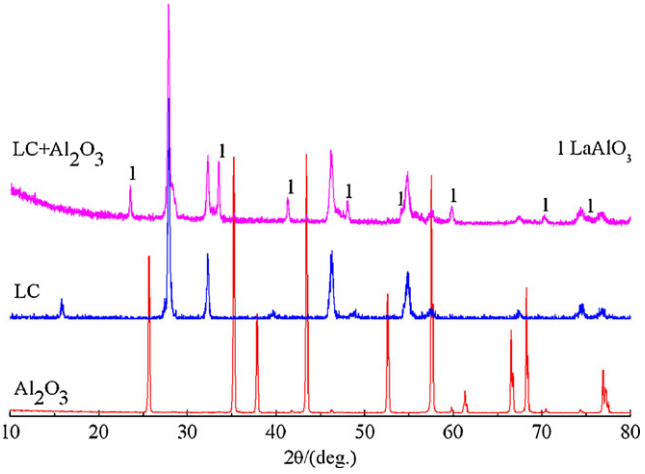

Fig. 4. XRD patterns of the mixture of LC and Al_2O_3 powders after being heated at 1373 K for 48 h.

4. Conclusions

The LZ, LZ7C3 and LC coatings were prepared by EB-PVD in this work. These coatings have slightly deviated from the theoretical values after deposition due to the different evaporation rates of oxides, and the deviation could be reduced by properly controlling the deposition condition. DCL-TBCs of LZ7C3 and LC could also be deposited with a single LZ7C3 ingot by properly controlling the deposition energy. The failure of LZ and LZ7C3 coatings is probably a result of the abnormal oxidation of bond coat, the mismatch thermal expansion coefficient of ceramic layer and bond coat and the visible cracks initiation, propagation and extension. Additionally, the sintering-induced of LZ7C3 coating, the extension of transverse cracks and the chemical incompatibility of LC and TGO seem to be the primary factors for the spallation of DCL coating.

Acknowledgements

Financial supports from projects NSFC-50825204, NSFC-20921002 and Hunan Provincial Key Laboratory of Materials

Protection for Electric Power and Transportation (Changsha University of Science & Technology) are also gratefully acknowledged.

References

[1] Y.H. Wang, J.H. Ouyang, Z.-G. Liu, J. Alloys Compd. 485 (2009) 734–738.
[2] Z.-G. Liu, J.H. Ouyang, Y. Zhou, J. Alloys Compd. 473 (2009) L17–L19.
[3] Z.-G. Liu, J.H. Ouyang, B.H. Wang, Y. Zhou, J. Li, J. Alloys Compd. 466 (2008) 39–44.
[4] Z.-G. Liu, J.H. Ouyang, Y. Zhou, J. Alloys Compd. 472 (2009) 319–324.
[5] X.Q. Cao, J. Mater. Sci. Technol. 23 (2007) 15–35.
[6] X.H. Zhong, Z.H. Xu, Y.F. Zhang, J.F. Zhang, X.Q. Cao, J. Alloys Compd. 469 (2009) 82–88.
[7] Z.-G. Liu, J.H. Ouyang, Y. Zhou, J. Li, J. Alloys Compd. 468 (2009) 350–355.
[8] H.F. Chen, Y.F. Gao, Y. Liu, H.J. Luo, J. Alloys Compd. 480 (2009) 843–848.
[9] Z.-G. Liu, J.H. Ouyang, Y. Zhou, J. Li, X.L. Xia, J. Eur. Ceram. Soc. 29 (2009) 647–652.
[10] B. Saruhan, P. Francois, K. Fritscher, U. Schulz, Surf. Coat. Technol. 182 (2004) 175–183.
[11] H.F. Chen, Y.F. Gao, S.Y. Tao, Y. Liu, H.J. Luo, J. Alloys Compd. 486 (2009) 391–399.
[12] W. Ma, S.K. Gong, H.B. Xu, X.Q. Cao, Surf. Coat. Technol. 200 (2006) 5113–5118.
[13] U. Schulz, B. Saruhan, K. Fritscher, C. Leyens, Int. J. Ceram. Technol. 1 (4) (2004) 302–315.
[14] X.Q. Cao, R. Vassen, W. Jungen, S. Schwartz, F. Tietz, D. Stöver, J. Am. Ceram. Soc. 84 (9) (2001) 2086–2090.
[15] U. Schulz, K. Fritscher, M. Peters, Surf. Coat. Technol. 82 (1996) 259–269.
[16] Z.H. Xu, L.M. He, X.H. Zhong, R.D. Mu, S.M. He, X.Q. Cao, J. Alloys Compd. 478 (2009) 168–172.
[17] W. Ma, S.K. Gong, H.F. Li, H.B. Xu, Surf. Coat. Technol. 202 (2008) 2704–2708.
[18] X. Wang, U. Helmersson, J. Birch, W. Ni, J. Cryst. Growth 171 (3–4) (1997) 401–408.
[19] Z.H. Xu, L.M. He, X.H. Zhong, J.F. Zhang, X.L. Chen, H.M. Ma, X.Q. Cao, J. Alloys Compd. 480 (2009) 220–224.
[20] H.B. Xu, S.K. Gong, L. Deng, Thin Solid Films 334 (1998) 98–102.